



1 **Intercomparison of in-situ NDIR and column FTIR**
2 **measurements of CO₂ at Jungfraujoch**

3

4 **Michael F. Schibig¹, Emmanuel Mahieu², Stephan Henne³, Bernard Lejeune²,**
5 **Markus C. Leuenberger¹**

6 [1] Climate and Environmental Physics, Physics Institute and Oeschger Centre for Climate
7 Change Research, University of Bern, Bern, Switzerland

8 [2] Institut d'Astrophysique et de Géophysique, Université de Liège, Liège, Belgique

9 [3] Empa, Swiss Federal Laboratories for Materials Testing and Research, Dübendorf,
10 Switzerland

11 Correspondence to: leuenberger@climate.unibe.ch

12 Keywords: CO₂, FTIR, NDIR, Jungfraujoch, intercomparison, CO₂ trend

13 **Abstract**

14 We compare two CO₂ time series measured at the High Alpine Research Station Jungfraujoch
15 (3580 m a.s.l., Switzerland) in the period from 2005 to 2013 with an in-situ surface
16 measurement system using a nondispersive infrared analyzer (NDIR) and a ground-based
17 remote sensing system using solar absorption Fourier Transform Infrared spectrometry
18 (FTIR). Although the two data sets show an absolute shift of about 13 ppm, the slopes of the
19 annual CO₂ increase are in good agreement within their uncertainties. They are 2.04 ± 0.07
20 ppm yr^{-1} and $1.97 \pm 0.05 \text{ ppm yr}^{-1}$ for the FTIR and the NDIR system, respectively. The
21 seasonality of the FTIR and the NDIR system is $4.46 \pm 1.11 \text{ ppm}$ and $10.10 \pm 0.73 \text{ ppm}$,
22 respectively. The difference is caused by a dampening of the CO₂ signal with increasing
23 altitude due to mixing processes. While the minima of both data series occur in the middle of
24 August, the maxima of the two datasets differ by about ten weeks, the maximum of the FTIR
25 measurements is in middle of January, whereas the maximum of the NDIR measurements is
26 found at the end of March. Sensitivity analyses revealed that the air masses measured by the
27 NDIR system at the surface of Jungfraujoch are mainly influenced by central Europe, whereas
28 the air masses measured by the FTIR system in the column above Jungfraujoch are influenced
29 by regions as far west as the Caribbean and the United States.



1 The correlation between the hourly averaged CO₂ values of the NDIR system and the
2 individual FTIR CO₂ measurements is 0.820, which is very encouraging given the largely
3 different sampling volumes. Further correlation analyses showed, that the correlation is
4 mainly driven by the annual CO₂ increase and to a lesser degree by the seasonality. Both
5 systems are suitable to monitor the long-term CO₂ increase, because this signal is represented
6 in the whole atmosphere due to mixing.

7

8 **1 Introduction**

9 CO₂ is the most important anthropogenic greenhouse gas, with a large contribution to the
10 greenhouse effect (Arrhenius, 1896) and an additional radiative forcing of the atmosphere
11 currently evaluated at 1.68 Wm⁻² (IPCC, 2013). The strength of the forcing is depending on
12 its atmospheric mole fraction which is ruled by the processes of the carbon cycle as well as by
13 anthropogenic CO₂ emissions from fossil fuel combustion and land use change. The major
14 reservoirs of the carbon cycle besides the lithosphere are the soils, the ocean, the biosphere
15 and the atmosphere, where the latter is also acting as the main link between the biosphere and
16 the ocean. The processes coupling the biosphere with the atmosphere are photosynthesis,
17 where CO₂ is used by plants to convert solar energy into chemical energy by producing
18 carbohydrates from CO₂ and H₂O, and respiration, the decomposition of biogenic
19 carbohydrates back into CO₂, H₂O and energy, where CO₂ is released back to the atmosphere.
20 The linking process between the atmosphere and the ocean is dissolution of CO₂ in oceanic
21 water, where it is subsequently chemically bound to bicarbonate and carbonate and therefore
22 removed from the carbon cycle on a longer timescale (Broecker and Peng, 1982; Feely et al.,
23 2004; Heinze et al., 1991; Sillén, 1966). The solution of CO₂ in water is depending on the
24 partial pressures of CO₂ in the atmosphere and the ocean, if the atmospheric partial pressure
25 of CO₂ above sea water is greater than the oceanic partial pressure of CO₂, CO₂ is taken up by
26 the seawater and vice versa. Other factors as e.g. salinity, temperature etc. affect the solubility
27 of CO₂ in seawater additionally (Bohr, 1899; Takahashi et al., 2009). Photosynthesis and
28 respiration, on the other hand, are mainly driven by climatic conditions of the environment. In
29 the northern hemisphere, especially in the extratropics with distinct seasons, the dominating
30 process in late spring, summer and fall is photosynthesis and thereby the uptake of CO₂ from
31 the atmosphere. In autumn respiration and with it the release of CO₂ from the biosphere into
32 the atmosphere starts to take over and is the ruling process in winter until spring when



1 photosynthesis becomes the dominating process again. Due to these alternating processes, the
2 CO₂ mole fraction in the atmosphere shows a seasonal cycle with its maximum generally in
3 early spring and its minimum in fall (Halloran, 2012; Keeling et al., 1976; Keeling et al.,
4 2001; Machida et al., 2002). A further component in the change of atmospheric CO₂ mole
5 fraction is CO₂ release due to fossil fuel combustion (Karl and Trenberth, 2003; Revelle and
6 Suess, 1957; Tans et al., 1990). Nowadays, roughly half of the anthropogenically produced
7 CO₂ ends up in the oceans and the biosphere, whereas the other half is accumulating in the
8 atmosphere and leads to a more or less steady increase of the atmospheric CO₂ mole fraction
9 (Bender et al., 2005; Le Quéré et al., 2013; Sabine et al., 2004). Measuring the atmosphere's
10 CO₂ mole fraction on the long-term is therefore important to understand the sources and sinks
11 of the carbon cycle and the annual CO₂ increase due to fossil fuel combustion and land use
12 change. To measure the evolution of CO₂ in the atmosphere on a global scale satellite remote
13 sensing methods can be used as e.g. OCO-2 (Crisp et al., 2004, Pollock et al., 2010,
14 Thompson et al., 2012) or GOSAT (Chevallier et al., 2009, Yokota et al., 2009) but they are
15 limited by e.g. cloud cover, temporal coverage due to the orbit, coarse resolution etc. An
16 intercomparison between GOSAT and several TCCON (Total Carbon Column Observation
17 Network) stations showed a mean difference for daily averages of -0.34 ± 1.37 ppm
18 (Heymann et al., 2015). Ground based measurement systems on the other hand have a high
19 temporal resolution and provide very accurate data, which can be used to validate satellite
20 data (Buchwitz et al., 2006; Butz et al., 2011; Dils et al., 2006; Morino et al., 2011; Wunch et
21 al., 2011) or as model input (Chevallier et al., 2010), but surface observations have often a
22 limited representativeness and are often influenced by nearby processes and hence, not
23 representative for larger areas. Also the influence of the biosphere or anthropogenic pollution
24 can be a serious issue and make it very challenging to measure background air. Therefore, to
25 measure global CO₂ trends the sampling site should be at a very remote place like e.g. Mace
26 Head Station (Bousquet et al., 1996; Messenger et al., 2008) on the western coast of Ireland or
27 the flask sampling network in the Pacific of NOAA (Komhyr et al., 1985; Trolier et al., 1996).
28 Another possibility is to measure in the free troposphere e.g. with airplanes as done in the
29 CARIBIC project (Brenninkmeijer et al., 2007) or the CONTRAIL project (Machida et al.,
30 2008) or at high altitudes which are mostly in the free troposphere as e.g. Mauna Loa
31 (Keeling et al., 1976; Keeling et al., 1995; Pales and Keeling, 1965; Thoning et al., 1989). The
32 High Alpine Research Station Jungfraujoch (JFJ) with its altitude of 3580 m a.s.l. (Sphinx



1 Observatory) and position mostly above the planetary boundary (Henne et al., 2010) is
2 therefore a very suitable spot to conduct ground based CO₂ background measurements.

3 The University of Liège (Belgium) has been measuring infrared radiation at JFJ since the
4 1950s and started regular FTIR (Fourier Transform InfraRed) measurements in 1984. The
5 Climate and Environmental Physics Division (KUP) of the University of Bern started
6 measuring CO₂ and δO₂/N₂ in 2000 by a flask sampling program and since the end of 2004,
7 CO₂ and O₂ have been additionally measured with a continuously operating system of a NDIR
8 instrument and a paramagnetic cell. In this study we compared the FTIR and the NDIR data
9 set to see if the two complementary measurement techniques are catching the same trends,
10 seasonalities and variations in atmospheric CO₂ mole fraction at and above Jungfraujoch.

11

12 **2 Methods**

13 **2.1 Measurement site**

14 The High Altitude Research Station Jungfraujoch (JFJ) is located 7°59'02'' E, 46°32'53'' N
15 at the northern margin of the Swiss Alps. The Jungfraujoch is a mountain saddle between the
16 Mönch (4099 m a.s.l.) and Jungfrau (4158 m a.s.l.) summits at a height of 3580 m a.s.l.
17 (Sphinx Observatory) and is accessible year-round by train. Because of the high elevation, the
18 station is usually above the planetary boundary layer (PBL) and therefore mainly receives air
19 from the free troposphere which is why it was classified as “mostly remote” by Henne et al.
20 (2010). Nevertheless, the station can be influenced by polluted air during specific events such
21 as frontal passages and Föhn (Uglietti et al., 2011; Zellweger et al., 2003) or thermal uplift of
22 polluted air from the surrounding valleys on fair weather days (Baltensperger et al., 1997;
23 Henne et al., 2005; Zellweger et al., 2000). Because of the high elevation, the accessibility and
24 the good infrastructure, the JFJ is an ideal location for in-situ measurements of atmospheric
25 background air from continental Europe (Baltensperger et al., 1997; Henne et al.,
26 2010; Zellweger et al., 2003). JFJ is also one of the currently 29 core sites of the WMO GAW
27 (Global Atmospheric Watch) programme.

28 **2.2 In-situ NDIR measurements at Jungfraujoch**

29 The KUP CO₂ measurements are based on a combined system to monitor CO₂ and O₂
30 changes in the atmosphere. The ambient air is entering through a strongly ventilated (600



1 m³ h⁻¹) common inlet on the observatory's roof to a manifold, which serves many trace gas
2 analyzers, where an aliquot of it is drawn to the KUP system. The air is cryogenically dried to
3 a dew point of -90 °C (FC-100D21, FTS systems, USA). Temperature as well as pressure is
4 stabilized to avoid influences caused by ambient air density fluctuations. This allows the
5 determination of CO₂ by a NDIR spectrometer (Maihak S710) with a frequency of 1 Hz and
6 O₂ by a paramagnetic cell under highly controlled conditions. Measurements are done in a
7 cyclic sequence of 18 hours with each gas measured for 6 minutes with only the last 115
8 seconds of a six minute period used for mole fraction determination, to allow for signal
9 stabilization after changing the sample source. At the beginning of each 18-hour sequence, the
10 system is calibrated with two reference gases (high and low span). A working gas is measured
11 between two ambient air measurements to correct for short term variations. All measurements
12 ending in a particular hour are used for the calculation of hourly mean CO₂ observations,
13 which in our case includes therefore 6 ambient observation values per hour. Cylinder
14 measurements with a known mole fraction showed a precision better than 0.04 ppm for 1 hour
15 analysis. The CO₂ values are reported on the WMO X2007 scale. A multi-annual
16 intercomparison between the NDIR system and a cavity ring-down spectroscope at JFJ
17 showed a very good agreement of the CO₂ measurements (Schibig et al., 2015).

18 **2.3 Column FTIR measurements at Jungfraujoch**

19 The University of Liège has been recording atmospheric solar spectra at JFJ since the early
20 1950s. The current FTIR instrument is a commercially available Bruker IFS-120 HR with a
21 resolution of up to 0.001 cm⁻¹ (Mahieu et al., 1997). It features interchangeable detectors, a
22 KBr beam-splitter and dedicated optical filters, which altogether give the possibility to cover
23 the 1 to 14 μm spectral range (Zander et al., 2008). Here gases such as CO₂, CH₄ and H₂O
24 show numerous absorption lines documenting contributions to the greenhouse effect. These
25 spectra also contain information about the abundance of many additional absorbing gas
26 species in the path between the instrument and the sun, essentially present either in the
27 troposphere or in the stratosphere. The CO₂ data set used here has been derived from the
28 reference total column time series produced within the framework of the NDACC monitoring
29 program (Network for the Detection of Atmospheric Composition Change; see
30 <http://www.ndacc.org>), presented previously in e.g. Zander et al. (2008; see Figure 6). The
31 uncertainty on the main CO₂ line strength is estimated at 2 to less than 5% in the HITRAN
32 compilation (Rothman et al., 2005), leading to a systematic error on the retrieved total column



1 of the same magnitude. In the meantime, the data set has been consistently updated, still
2 using the SFIT-1 algorithm (version 1.09c) and a single microwindow spanning the 2024.3 –
3 2024.7 cm^{-1} spectral interval, whose main spectral line is coming from $^{13}\text{CO}_2$. The single CO_2
4 a priori vertical distribution used in all retrievals is characterized by a constant mixing ratio of
5 338 ppm from the surface up to the tropopause, then slightly decreasing to stabilize at 330
6 ppm at 20 km and above. A simple scaling retrieval is performed, and the mixing ratio
7 derived for the troposphere is used in the present comparisons. Note that the
8 representativeness of this unique profile is not optimal for all seasons and may lead to an
9 underestimation of the seasonal amplitude (see Fig. 1 in Barthlott et al., 2015), because of a
10 non-optimum vertical sensitivity of the FTIR retrieval. Indeed, typical values of the total
11 column averaging kernel – indicative of the fraction of information coming from retrieval
12 rather than from the a priori (e.g. Vigouroux et al., 2015) – are in the 0.5 – 1 range between
13 the ground and 10 km altitude, in line with Fig. 4 of Barthlott et al. (2015).

14 **2.4 Data processing**

15 The NDIR data set is much more influenced by near ground processes like thermal uplift of
16 PBL air from the surrounding valleys, advection of PBL air by synoptic events etc. than the
17 FTIR and shows therefore a higher variability. Additionally, because of the large volume of
18 the column sampled by the FTIR above JFJ the CO_2 mole fraction measured by the FTIR is
19 averaged and the data set is far less sensitive to local events than the in-situ NDIR
20 measurements. The FTIR needs a cloudless sky to be able to measure, whereas the NDIR
21 system is measuring under all conditions, which can lead to very high CO_2 mole fractions
22 during e.g. Föhn events, when the sky is cloudy and polluted air from the heavily
23 industrialized Po basin (Northern Italy) is advected to JFJ. Therefore, only measurements of
24 background air should be taken into account to compare the two data sets properly.

25 **2.4.1 Filtering, trend and seasonality calculation**

26 The background data were selected using a statistical approach. A cubic spline was fitted to
27 both datasets individually, the standard deviation of the residuals was calculated and all points
28 beyond 2.7σ were flagged as outliers. This process was repeated in both data sets until
29 convergence. The threshold of 2.7σ was chosen because in normally distributed data more
30 than 99 % of the total data points would be included for further calculations and only the most
31 obvious outliers (less than 1 %) would be rejected.



1 The CO₂ mole fraction is dominated by two major processes. One is the linear increase due to
2 fossil fuel combustion (trend) and one is the annual in- and decrease due to respiration and
3 photosynthesis (seasonality). The trend was calculated for both datasets individually with a
4 Monte Carlo approach.

5 For the trend calculation we intentionally used the datasets including seasonal signals because
6 it leads to realistic trend error estimates compared to deseasonalized datasets, which in our
7 view tend to underestimate the error. The datasets were split in two subsets, where each of the
8 subsets spanned over $n - 0.5$ phases (in this study n equals 9 years) to prevent a bias in the
9 trend calculation due to the seasonal cycle. The first subsets start in January 2005, the second
10 subsets start in July 2005. In each subset about 2 % (a higher number does improve the result)
11 of the points were selected randomly and the linear trend was calculated. This was repeated
12 500 times with each subset and the averages of these linear trends were taken as the slopes of
13 the datasets.

14 To calculate the seasonality, the two datasets were detrended and monthly averages were
15 formed, from which the seasonality was calculated as the difference between the highest and
16 the lowest value.

17 **2.4.2 Correlation analysis**

18 Because of the different time resolutions for in-situ and FTIR measurements we selected
19 those in-situ measurements (six minute and hourly NDIR averages) that are closest (± 30 min)
20 to the FTIR values for correlation analysis.

21 Since the differences between both correlation analyses were negligible (see results section),
22 it was decided to continue with the hourly averages of the NDIR dataset only, which is the
23 common output of the NDIR database.

24 The FTIR's sample volume is much bigger than the NDIR system's and because of
25 transportation processes there's a possibility of mixing processes. To check, a moving average
26 of the NDIR data with increasing width was calculated to see if the correlation is enhanced
27 with expanding width (from 0 to ± 600 h).

28 Furthermore, the column measurements were retrieved for the layer between 3.58 km (altitude
29 of the Sphinx Observatory) to the top atmosphere (set to 100 km in the retrieval scheme)
30 whereas the NDIR system is measuring at the lower boundary of the FTIR's sampling
31 column, therefore it is possible that a time shift in the measured CO₂ mole fractions due to
32 advection, uplift of air parcels etc. occurs. To check whether a systematic time shift exists



1 between the two datasets, the NDIR measurements were shifted relative to the FTIR data
2 from -60 to +60 days (corresponding to -1440 h to +1440 h) in hourly steps and again the
3 correlation of the two data sets was calculated. If there is a systematic time shift, the deviation
4 should be indicated by increased correlation values.

5 **2.5 FLEXPART model runs**

6 From 2009 to 2011, backward Lagrangian particle dispersion model simulations were
7 performed with FLEXPART (Stohl, et al. 2005) to simulate the transport towards JFJ and
8 estimate surface source sensitivities (footprints) of the sampled air masses. To account for the
9 complex flow in the Alpine area, a regional scale version of the model driven by operational
10 output from the regional scale numerical weather prediction model COSMO as produced by
11 MeteoSwiss was used (Henne et al., 2015, Oney et al., 2015) . Since COSMO is a limited area
12 model, the transport of particles leaving the domain was further simulated in the global scale
13 version of FLEXPART (Stohl et al., 2005) driven by operational analysis fields of the
14 European Centre for Medium Range Weather Forecast (ECMWF). In the Alpine area,
15 COSMO input data had a horizontal resolution of approximately 2 km x 2 km, in Western
16 Europe 7 km x 7 km. Of the 1214 FTIR measurements in this period, footprints were
17 available for 766. The model simulated footprints of the surface in-situ observations and five
18 partial columns above JFJ reaching from 3365-4226 m a.s.l., 4226-4912 m a.s.l., 4912-5629
19 m a.s.l., 5629-6386 m a.s.l. and 6386-7184 m a.s.l. The lower boundary is below JFJ in order
20 to account for smoothed model topography. Particles released at and above JFJ were followed
21 10 days backward in time to calculate source sensitivities. Source sensitivities were evaluated
22 on regular longitude/latitude grids. The resolution was 0.5° x 0.5° globally, 0.2° x 0.2° over
23 Europe and an even higher resolution of 0.1° x 0.1° was used in the Alpine area. The
24 footprints of the individual measurements of each partial column were averaged to monthly
25 means to get information about the origin of the air masses in the according month (Henne,
26 2014;Henne et al., 2013).

27

28 **3 Results**

29 Because of the different measurement techniques, the number of data points in the two
30 datasets is different. In the period 2005 to 2013 the NDIR dataset contains 68477 hourly
31 averages from which about 5 % were omitted as pollution or depletion events resulting from



1 PBL influence as estimated by the filtering (Figure 1). In the same period, the FTIR dataset
2 shows 3068 measurements of which about 5 % were rejected as pollution and depletion
3 events, too (Figure 2). For all further calculations, only the filtered datasets were used.
4 The average of the detrended and deseasonalized NDIR data before and after filtering was
5 0.00 ± 2.65 ppm and 0.00 ± 1.84 ppm (Figure 3 A), the average of the FTIR data was $0.01 \pm$
6 2.61 ppm and 0.01 ± 2.16 ppm, respectively (Figure 3 B).
7 With a Monte Carlo algorithm, the values of the annual change of the CO₂ mole fraction of
8 the two datasets were calculated. Despite the shift between the two datasets of roughly 13
9 ppm (i.e. about 3%, in line with the systematic uncertainty affecting the FTIR measurement;
10 see section 2.3) and the different measurement techniques the annual CO₂ increase is quite
11 similar. The FTIR slope is 2.04 ± 0.07 ppm yr⁻¹ and the NDIR dataset shows a slope of $1.97 \pm$
12 0.05 ppm yr⁻¹, so they are equal within their uncertainties (Figure 4).
13 By detrending the datasets with the derived slopes, the seasonality can be calculated. The
14 column dataset shows a seasonality of 4.46 ± 1.11 ppm whereas the in-situ measurements at
15 the Sphinx Observatory show a seasonality roughly twice as big, namely 10.10 ± 0.73 ppm. To
16 find the moment of the average minima and maxima, a two harmonic fit function was applied
17 to the detrended datasets. The minima of the FTIR and NDIR datasets are both in the middle
18 of August, but the maxima are roughly ten weeks apart. The maximum of the NDIR datasets
19 occurs at the end of March, whereas seasonality of the FTIR dataset already reaches its
20 maximum in the middle of January (Figure 5).
21 The footprints of August, January and March, when the extrema of the seasonal cycle
22 occurred, as calculated with FLEXPART show that the in-situ observation at Jungfraujoch is
23 mainly receiving air masses that are influenced by Central Europe, and to a lesser degree by
24 the Mediterranean area and the northern Atlantic (Figure 6, Figure 7 and Figure 8).
25 With increasing altitude, the footprints of the sub-columns indicate, that the measured air
26 masses become more sensitive to regions as far west as e.g. the Caribbean and the United
27 States and that the influence from the European continent and northern regions higher than
28 50°N is decreasing (Figure 6, Figure 7 and Figure 8).
29 To estimate the relationship between the FTIR and NDIR measurements the correlation was
30 calculated. The FTIR measurements take normally about 10 min and are done whenever
31 possible. Therefore the FTIR data is reported exactly at the measuring time. The NDIR on the
32 other hand is measuring non-stop, but only 115 s of six-minute intervals (see methods) are
33 used to calculate a data point and the six-minute data is normally averaged to hourly averages.



1 Therefore we first checked whether the high resolution data are necessary or hourly data is
2 good enough. To do so, to each FTIR data point the nearest high resolution and hourly
3 averaged NDIR values were assigned. An additional condition was that the NDIR value must
4 not be further apart than ± 30 min, otherwise no NDIR data point was set, which was the case
5 in about 10 % of the FTIR data points. The correlation between the FTIR and the high
6 resolution NDIR CO₂ measurements and between the FTIR and the hourly averages were
7 calculated to be 0.819 and 0.820, so the differences between the two regression values are
8 negligible. To examine the relationship between the FTIR and the NDIR measurements
9 further, the seasonality of the two datasets was eliminated which gave almost the same
10 correlation of 0.824 (0.838 with the high resolution data). In the next step only the trend was
11 subtracted and the remaining seasonalities were compared, which lead to a much smaller
12 correlation of 0.460 (0.461 with the high resolution data). In a final step, the trend as well as
13 the seasonality was removed, which resulted in a correlation of 0.071 (0.084 high resolution
14 data vs. FTIR). Since correlations between the FTIR data and the NDIR's high resolution and
15 the hourly data were almost the same, only the hourly data was considered for further
16 calculations (Figure 9).

17 As mentioned above, the column measurements represent the whole vertical distribution
18 above Jungfraujoch whereas the NDIR system is measuring at the base of the FTIR's
19 sampling column. Therefore, the two records might be time-delayed due to advection, uplift
20 of air parcels etc. To check for a potential time lag, the NDIR measurements were shifted
21 relative to the FTIR data from -1440 to +1440 hours in hourly steps.

22 The correlations between the NDIR and FTIR datasets and between the deseasonalized NDIR
23 and FTIR datasets show a peak region at a time shift from -10 h to 60 h with the highest
24 correlation being 0.830 and 0.836 respectively (Figure 10 A, Figure 10 B). The correlation
25 between the datasets is decreasing before and after this range, in the deseasonalized datasets
26 the correlation stays more or less stable. The correlation between the two trend corrected
27 datasets shows a plateau of enhanced correlation values from -50 h to 200 h time shift with a
28 maximum correlation of 0.495 at a time shift of 165 h, at lower and higher time shifts, the
29 correlation is decreasing (Figure 10 C). The correlation of the detrended and deseasonalized
30 datasets shows no distinct pattern and is oscillating around 0 (Figure 10 D).

31 Since the air volume measured by the FTIR is much bigger than the NDIR system's volume,
32 vertical mixing and transport processes can occur and thereby changing the CO₂ mole fraction
33 in the measured air parcels. Therefore moving averages with increasing widths (up to ± 600 h)



1 were calculated from the NDIR data and the obtained averaged NDIR values were correlated
2 with the filtered FTIR dataset. Changing the width of the moving average doesn't have a
3 strong influence on the correlation between the two filtered datasets, because the increasing
4 width of the moving average just smooths the dataset. The correlation remains at about 0.85
5 (Figure 11 A), with a very small increase of the correlation at the beginning, most probably
6 due to the above mentioned smoothing effect. The same is true for the correlation between the
7 deseasonalized datasets. They show high correlation of about 0.84 over the whole range of
8 widths, with a slight increase at the beginning, which is not significant (Figure 11 B). By
9 detrending the datasets, the correlation is increasing with the width of the moving average and
10 shows a plateau of higher correlation of about 0.5 at a width 150 to 600 h from where on it is
11 decreasing again (Figure 11 C). However, the changes in the correlation within the range of
12 150 h to 600 h are very small. The detrended and deseasonalized datasets show a very low
13 correlation and the improvement of the correlation due to the changing width of the moving
14 average is negligible. Over all, the improvement of the correlations due to the changing width
15 of the moving average is very small (Figure 11 D).

16 Finally both, the time shift and the width of the moving average were varied about ± 1440 h
17 and ± 600 h, to see with which combination of time shift and width the best correlation can be
18 reached. They all show a ridge of higher correlation at a time shift around zero which is
19 broadening with increasing width of the moving average, except for the data without slope
20 and seasonality, which have a low correlation anyway (Figure 12). The increasing width of
21 the moving average leads to a small improvement of the correlations in the beginning,
22 however over all it doesn't seem to have a strong influence on the correlations. The time shift
23 on the other hand has an influence on correlation between the complete filtered datasets and
24 even more on the correlation of the detrended datasets. In the correlation of the
25 deseasonalized datasets, the influence of the time shift is very limited except for the small
26 ridge of slightly enhanced correlations around zero time shift as mentioned above.

27

28 **4 Discussion**

29 The filtered FTIR and NDIR datasets show a very similar increase in the CO₂ mole fraction of
30 ambient air, despite the two totally different measurement principles. The calculated annual
31 CO₂ trends of the FTIR and NDIR datasets are 2.04 ± 0.07 ppm yr⁻¹ and 1.97 ± 0.05 ppm yr⁻¹
32 respectively (Figure 4) and are in good agreement with flask measurements done at JFJ with a



1 slope of 1.85 ppm yr^{-1} (van der Laan-Luijkx et al., 2013) and other remote stations in the
2 northern hemisphere; for example Mauna Loa with 2.05 ppm yr^{-1} (Tans and Keeling, 2014) or
3 Alert with 1.85 ppm yr^{-1} (Keeling et al., 2001). Also the NDIR dataset's average seasonality
4 of $10.10 \pm 0.73 \text{ ppm}$ is in good agreement with the seasonality of these flask measurements,
5 which were $10.54 \pm 0.18 \text{ ppm}$ in the period 2007 to 2011 (van der Laan-Luijkx et al., 2013)
6 and is roughly double the FTIR's average seasonality of $4.46 \pm 1.11 \text{ ppm}$ (Figure 5). The
7 lower seasonality of the FTIR dataset can be explained by the fact that the NDIR system is
8 measuring CO_2 mole fractions at the Sphinx Observatory, which is most of the time above the
9 PBL (Henne et al., 2010) but still closer to the ground than the FTIR measurements.
10 Therefore the signal of the biosphere is stronger than in the column, where it is attenuated by
11 vertical mixing and transport processes of the atmosphere with increasing height. Also the
12 fixed a priori vertical CO_2 profile may contribute partly to the lower seasonality of the FTIR
13 measurements. The shape of the profile used to retrieve the CO_2 data doesn't reproduce the
14 changes due to seasonality and is therefore not always the optimum. By using a seasonally
15 varying a priori retrieval the seasonality might be slightly higher because the amplitude of
16 CO_2 is better retrieved (Barthlott et al., 2015). Furthermore, in the tropopause and the lower
17 stratosphere, the phase of the CO_2 seasonality is shifted by several months (Bönisch et al.,
18 2008; Gurk et al., 2008; Bönisch et al., 2009). However, this has only a minor influence on the
19 observed dampening of the amplitude of the FTIR seasonality compared to the vertical
20 mixing, since the stratosphere contains only about 10 % of the abundance of atmospheric air
21 molecules.

22 It is not easy to define the seasonal minimum and maximum in the FTIR dataset because they
23 are not very clearly pronounced. By fitting a two harmonic function the minimum was found
24 to be in the middle of August, the maximum in the middle of January. While the minimum of
25 the NDIR dataset is around the same time, the maximum of the FTIR dataset occurs roughly
26 ten weeks earlier than the maxima of the NDIR dataset (Figure 5). The timing of the minima
27 of both datasets and the maximum of the NDIR dataset coincide quite well with net land-
28 atmosphere carbon flux changes from negative to positive values and vice versa (Zeng et al.,
29 2014). Therefore an alternative explanation is needed for the early maximum of the FTIR
30 dataset. Sensitivity analyses revealed that the upper tropospheric air originates from lower
31 latitudes than the in-situ air measured by the NDIR. Therefore the air measured by the FTIR
32 is partially decoupled from the increasing CO_2 values of the winter-time northern hemisphere.
33 Furthermore, the decoupling might be amplified by the weak overturn of tropospheric air in



1 winter. Towards spring, the tropospheric overturn speeds up again which results in
2 synchronous CO₂ minima for both datasets in August. Similar studies investigating CO at JFJ
3 also showed that JFJ is not only sensitive to Central Europe but also to regions as far west as
4 for example North America, the Pacific or even Asia and that the influence of these regions is
5 getting stronger with increasing height (Dils et al., 2011; Pfister et al., 2004; Zellweger et al.,
6 2009). Additionally, the assumption of a fixed a priori CO₂ vertical distribution to retrieve the
7 column integrated CO₂ concentration from the FTIR dataset may contribute partially to the
8 observed shift of ten weeks in the NDIR and FTIR maxima, because it is representing the
9 distribution in winter/spring inadequately.

10 Another hint that the two systems are not measuring the same air parcels can be found in
11 correlation analyses. After omitting outliers, which are mostly caused by synoptic events,
12 thermal uplift of polluted air from surrounding valleys, or other local to regional transport
13 events, the correlation of the two datasets is as large as 0.820, which is quite encouraging
14 considering the different nature of the measurements. By excluding the seasonality from both
15 datasets, the correlation stays almost the same, namely 0.824 but drops to 0.460 if the
16 seasonality is included but the annual CO₂ increase is subtracted. The comparison of the two
17 CO₂ datasets with the annual CO₂ increase and the seasonality subtracted showed a very low
18 correlation of 0.071, which is negligible (Figure 9). Because of possible delays and mixing
19 effects of the CO₂ signal, the time shift as well as the width of the moving average calculated
20 on the hourly values of the NDIR CO₂ values was varied between ± 1440 h and up to ± 600 h,
21 respectively. Shifting the NDIR time relative to the FTIR measurement time creates a ridge of
22 higher correlations around 0 h time shift with a slight tendency towards positive values
23 (Figure 12 A). This ridge-like form is clearly pronounced in the correlation plot between the
24 complete filtered FTIR and NDIR datasets and even more in the datasets without slope
25 (Figure 12 C) than in the correlation of the datasets without seasonality (Figure 12 B). There
26 it is very small and the correlation is high across the whole time shift and averaging width.
27 The constantly high correlation for deseasonalized datasets is due to both datasets containing
28 mostly background air whose CO₂ mole fraction changes are mainly driven by the annual CO₂
29 increase and by the seasonality of the CO₂ signal. Since the larger of the two, the seasonality,
30 is subtracted the high correlation is mainly driven by the slope which was calculated to be the
31 same within uncertainties and stays more or less constant over the examined period.
32 Therefore, the time shift has almost no influence. The remaining fluctuations in the CO₂ mole
33 fractions with higher frequencies than the seasonality seem to play a minor role, because



1 they're almost not visible in the comparison of the datasets without seasonality except for the
2 small ridge (Figure 12 B), or there's no correlation at all, as in the comparison of the two
3 datasets without slope and seasonality (Figure 12 D). This is indicating that the two
4 measurement systems are not measuring the same air parcels, even not with a certain delay, or
5 that the CO₂ signal of the NDIR system which is measured at the lower end of the FTIR
6 column becomes diluted beyond recognition for FTIR by the air mixing processes. The
7 positive effect of the increasing width of the moving average on the correlation is strongest,
8 but still very low, around the first 100 h. Afterwards its main effect is broadening the ridge of
9 the slightly enhanced correlations. The reason for the broadening effect of the increasing
10 width is its smoothing effect on the NDIR values. With increasing width, the influence of a
11 specific NDIR point on the correlation becomes smaller and the NDIR dataset evolves into a
12 smooth sine like curve with decreasing amplitudes, similar to the FTIR dataset, where this
13 form is caused by the higher sampling volume and the dampening due to mixing processes in
14 the atmosphere. However, the small influence of the moving average's width on the
15 correlation means that the correlation of the in-situ and the column measurement is mainly
16 influenced by the slope and the seasonality. Short term fluctuations play a minor role mainly
17 because either their CO₂ signal is dampened too much to be seen in the column measurement
18 or it is not measured at all as e.g. diurnal cycles because of the applied measurement methods.
19

20 **5 Conclusions**

21 Two datasets of CO₂ measurements at the High Altitude Research Station Jungfraujoch in the
22 period 2005 to 2013 were compared. The FTIR system is measuring the attenuation of solar
23 light at different wavelengths caused by molecules of light absorbing gas species in the
24 column between the Sphinx Observatory and the sun. From the obtained spectra, with the
25 knowledge of CO₂ specific extinction bands and the pressure distribution along the path of the
26 light, it is possible to calculate the CO₂ mole fraction in the column. The NDIR system is
27 measuring the CO₂ mole fraction of ambient air at the Sphinx Observatory which corresponds
28 to the lower boundary of the FTIR measurements. The two datasets were filtered with a
29 statistical approach to exclude CO₂ measurements which were influenced by recent transport
30 from the planetary boundary layer. The filtering caused a loss of about 5 % in both, the NDIR
31 and the FTIR dataset.



1 The annual CO₂ increase of the two datasets was calculated with a Monte Carlo approach.
2 Despite an average offset of 13 ppm between the two datasets, which is within the systematic
3 uncertainty affecting the FTIR measurement, the slopes were in good agreement, namely 2.04
4 ± 0.07 ppm yr⁻¹ in the FTIR measurements and 1.97 ± 0.05 ppm yr⁻¹ in the NDIR dataset. The
5 seasonality of the CO₂ signal of the NDIR and the FTIR system is 10.10 ± 0.73 ppm and 4.46
6 ± 1.11 ppm, respectively. The difference is caused by a dampening of the CO₂ signal with
7 increasing altitude due to mixing processes. While the minima of the two datasets both occur
8 in the simultaneously, the maxima of the FTIR dataset was found ten weeks earlier than the
9 NDIR maxima.

10 The difference in the occurrence of the minima is most probably caused by the different
11 transport history of the air masses measured at JFJ and in the column above JFJ. In January,
12 the in-situ system is measuring air from central Europe and the Mediterranean, whereas the
13 air masses of the column measurements are more affected by the subtropic Northern Atlantic.
14 With the onset of spring in Europe, the photosynthetic activity is increasing and the CO₂ mole
15 fraction of air measured by the in-situ system starts to decrease at the end of March. The two
16 filtered datasets as well as the two deseasonalized datasets show a high correlation, whereas
17 the correlation between the two detrended datasets is only mediocre and inexistent in the
18 between the two detrended and deseasonalized datasets. Neither shifting the time of the NDIR
19 measurements relative to the FTIR measurements nor increasing the width of the moving
20 average did increase the correlation between the two datasets significantly. The enhanced
21 correlation values around a time shift of zero indicates that (i) there isn't a systematic time
22 shift apparent and that (ii) the correlation between the two datasets is mainly driven by the
23 annual CO₂ increase and to a lesser degree by the seasonality. Therefore both measurement
24 systems are suitable to measure the annual CO₂ increase, because this signal is well mixed
25 within the atmosphere. Short term variations as the seasonality or daily variations are less or
26 not comparable, because (a) the transport history of the air parcels measured is different, (b)
27 the signal is mixed beyond recognition or (c) since the FTIR retrievals has little vertical
28 sensitivity the measured column signal contains mixed information from the troposphere and
29 the stratosphere.

30

31 **Acknowledgements**

32



1 This work was financially supported by the Swiss National Science Foundation (SNF-Project
2 200020_134641) and the Federal Office of Meteorology and Climatology MeteoSwiss in the
3 framework of Swiss GCOS. We like to thank the International Foundation High Altitude
4 Research Stations Jungfrauoch and Gornergrat (HFSJG), especially the custodians Martin
5 Fischer, Felix Seiler and Urs Otz for changing the calibration gases cylinders of the NDIR
6 system and other maintenance work. Additionally the authors like to thank Hanspeter Moret
7 and Peter Nyfeler for his precious work and help in maintaining and repairing the systems in
8 the Laboratory in Bern and also at Jungfrauoch. The Belgian contribution to the present work
9 was mainly supported by the Belgian Science Policy Office (BELSPO) and the Fonds de la
10 Recherche Scientifique – FNRS, both in Brussels. FLEXPART simulations were carried out
11 in the framework of EC FP7 project NORS (grant agreement N° 284421). Additional support
12 was provided by MeteoSwiss (GAW-CH) and the Fédération Wallonie Bruxelles. We are
13 grateful to the many colleagues and collaborators who have contributed to FTIR data
14 acquisition.

15



1 **References**

- 2 Arrhenius, S.: XXXI. On the influence of carbonic acid in the air upon the temperature of the
3 ground, *Philosophical Magazine Series 5*, 41, 237-276, 10.1080/14786449608620846, 1896.
- 4 Baltensperger, U., Gäggeler, H. W., Jost, D. T., Lugauer, M., Schwikowski, M., Weingartner,
5 E., and Seibert, P.: Aerosol climatology at the high-alpine site Jungfraujoch, Switzerland,
6 *Journal of Geophysical Research: Atmospheres*, 102, 19707-19715, 10.1029/97JD00928,
7 1997.
- 8 Barthlott, S., Schneider, M., Hase, F., Wiegele, A., Christner, E., González, Y., Blumenstock,
9 T., Dohe, S., García, O. E., Sepúlveda, E., Strong, K., Mendonca, J., Weaver, D., Palm, M.,
10 Deutscher, N. M., Warneke, T., Notholt, J., Lejeune, B., Mahieu, E., Jones, N., Griffith, D.
11 W. T., Velazco, V. A., Smale, D., Robinson, J., Kivi, R., Heikkinen, P. and Raffalski, U.:
12 Using XCO₂ retrievals for assessing the long-term consistency of NDACC/FTIR data sets,
13 *Atmospheric Measurement Techniques*, 8(3), 1555–1573, doi:10.5194/amt-8-1555-2015,
14 2015.
- 15 Bender, M. L., Ho, D. T., Hendricks, M. B., Mika, R., Battle, M. O., Tans, P. P., Conway, T.
16 J., Sturtevant, B., and Cassar, N.: Atmospheric O₂/N₂ changes, 1993–2002: Implications for
17 the partitioning of fossil fuel CO₂ sequestration, *Global Biogeochemical Cycles*, 19, GB4017,
18 10.1029/2004GB002410, 2005.
- 19 Bohr, C.: Definition und Methode zur Bestimmung der Invasions- und Evasionscoefficienten
20 bei der Auflösung von Gasen in Flüssigkeiten. Werthe der genannten Constanten sowie der
21 Absorptionscoefficienten der Kohlensäure bei Auflösung in Wasser und in
22 Chlornatriumlösungen, *Annalen der Physik Leipzig*, 62, 26, 1899.
- 23 Bönisch, H., Hoor, P., Gurk, C., Feng, W., Chipperfield, M., Engel, A., and Bregman, B.:
24 Model evaluation of CO₂ and SF₆ in the extratropical UT/LS region, *Journal of Geophysical*
25 *Research: Atmospheres*, 113, 10.1029/2007JD008829, 2008.
- 26 Bönisch, H., Engel, A., Curtius, J., Birner, T., and Hoor, P.: Quantifying transport into the
27 lowermost stratosphere using simultaneous in-situ measurements of SF₆ and CO₂, *Atmos.*
28 *Chem. Phys.*, 9, 5905-5919, 10.5194/acp-9-5905-2009, 2009.
- 29 Bousquet, P., Gaudry, A., Ciais, P., Kazan, V., Monfray, P., Simmonds, P. G., Jennings, S.
30 G., and O'Connor, T. C.: Atmospheric CO₂ concentration variations recorded at Mace Head,



- 1 Ireland, from 1992 to 1994, *Physics and Chemistry of the Earth*, 21, 477-481,
2 [http://dx.doi.org/10.1016/S0079-1946\(97\)81145-7](http://dx.doi.org/10.1016/S0079-1946(97)81145-7), 1996.
- 3 Brenninkmeijer, C. A. M., Crutzen, P., Boumard, F., Dauer, T., Dix, B., Ebinghaus, R.,
4 Filippi, D., Fischer, H., Franke, H., Frieß, U., Heintzenberg, J., Helleis, F., Hermann, M.,
5 Kock, H. H., Koeppel, C., Lelieveld, J., Leuenberger, M., Martinsson, B. G., Miemczyk, S.,
6 Moret, H. P., Nguyen, H. N., Nyfeler, P., Oram, D., O'Sullivan, D., Penkett, S., Platt, U.,
7 Pupek, M., Ramonet, M., Randa, B., Reichelt, M., Rhee, T. S., Rohwer, J., Rosenfeld, K.,
8 Scharffe, D., Schlager, H., Schumann, U., Slemr, F., Sprung, D., Stock, P., Thaler, R.,
9 Valentino, F., van Velthoven, P., Waibel, A., Wandel, A., Waschitschek, K., Wiedensohler,
10 A., Xueref-Remy, I., Zahn, A., Zech, U., and Ziereis, H.: Civil Aircraft for the regular
11 investigation of the atmosphere based on an instrumented container: The new CARIBIC
12 system, *Atmos. Chem. Phys.*, 7, 4953-4976, 10.5194/acp-7-4953-2007, 2007.
- 13 Broecker, W. S., and Peng, T.-H.: *Tracers in the Sea*, Lamont-Doherty Geological
14 Observatory, Palisades, New York, 1982.
- 15 Buchwitz, M., de Beek, R., Noël, S., Burrows, J. P., Bovensmann, H., Schneising, O.,
16 Khlystova, I., Bruns, M., Bremer, H., Bergamaschi, P., Körner, S., and Heimann, M.:
17 Atmospheric carbon gases retrieved from SCIAMACHY by WFM-DOAS: version 0.5 CO
18 and CH₄ and impact of calibration improvements on CO₂ retrieval, *Atmos. Chem. Phys.*, 6,
19 2727-2751, 10.5194/acp-6-2727-2006, 2006.
- 20 Butz, A., Guerlet, S., Hasekamp, O., Schepers, D., Galli, A., Aben, I., Frankenberg, C.,
21 Hartmann, J. M., Tran, H., Kuze, A., Keppel-Aleks, G., Toon, G., Wunch, D., Wennberg, P.,
22 Deutscher, N., Griffith, D., Macatangay, R., Messerschmidt, J., Notholt, J., and Warneke, T.:
23 Toward accurate CO₂ and CH₄ observations from GOSAT, *Geophysical Research Letters*, 38,
24 10.1029/2011GL047888, 2011.
- 25 Crisp, D., Atlas, R. M., Breon, F. M., Brown, L. R., Burrows, J. P., Ciais, P., Connor, B. J.,
26 Doney, S. C., Fung, I. Y., Jacob, D. J., Miller, C. E., O'Brien, D., Pawson, S., Randerson, J.
27 T., Rayner, P., Salawitch, R. J., Sander, S. P., Sen, B., Stephens, G. L., Tans, P. P., Toon, G.
28 C., Wennberg, P. O., Wofsy, S. C., Yung, Y. L., Kuang, Z., Chudasama, B., Sprague, G.,
29 Weiss, B., Pollock, R., Kenyon, D., and Schroll, S.: The Orbiting Carbon Observatory (OCO)
30 mission, *Advances in Space Research*, 34, 700-709,
31 <http://dx.doi.org/10.1016/j.asr.2003.08.062>, 2004.



- 1 Chevallier, F., Maksyutov, S., Bousquet, P., Bréon, F.-M., Saito, R., Yoshida, Y., and Yokota,
2 T.: On the accuracy of the CO₂ surface fluxes to be estimated from the GOSAT observations,
3 Geophysical Research Letters, 36, n/a-n/a, 10.1029/2009GL040108, 2009.
- 4 Chevallier, F., Ciais, P., Conway, T. J., Aalto, T., Anderson, B. E., Bousquet, P., Brunke, E.
5 G., Ciattaglia, L., Esaki, Y., Fröhlich, M., Gomez, A., Gomez-Pelaez, A. J., Haszpra, L.,
6 Krummel, P. B., Langenfelds, R. L., Leuenberger, M., Machida, T., Maignan, F., Matsueda,
7 H., Morguá, J. A., Mukai, H., Nakazawa, T., Peylin, P., Ramonet, M., Rivier, L., Sawa, Y.,
8 Schmidt, M., Steele, L. P., Vay, S. A., Vermeulen, A. T., Wofsy, S., and Worthy, D.: CO₂
9 surface fluxes at grid point scale estimated from a global 21 year reanalysis of atmospheric
10 measurements, Journal of Geophysical Research: Atmospheres, 115, D21307,
11 10.1029/2010JD013887, 2010.
- 12 Dils, B., De Mazière, M., Müller, J. F., Blumenstock, T., Buchwitz, M., de Beek, R.,
13 Demoulin, P., Duchatelet, P., Fast, H., Frankenberg, C., Gloudemans, A., Griffith, D., Jones,
14 N., Kerzenmacher, T., Kramer, I., Mahieu, E., Mellqvist, J., Mittermeier, R. L., Notholt, J.,
15 Rinsland, C. P., Schrijver, H., Smale, D., Strandberg, A., Straume, A. G., Stremme, W.,
16 Strong, K., Sussmann, R., Taylor, J., van den Broek, M., Velazco, V., Wagner, T., Warneke,
17 T., Wiacek, A., and Wood, S.: Comparisons between SCIAMACHY and ground-based FTIR
18 data for total columns of CO, CH₄, CO₂ and N₂O, Atmos. Chem. Phys., 6, 1953-1976,
19 10.5194/acp-6-1953-2006, 2006.
- 20 Dils, B., Cui, J., Henne, S., Mahieu, E., Steinbacher, M., and De Mazière, M.: 1997–2007 CO
21 trend at the high Alpine site Jungfraujoch: a comparison between NDIR surface in situ and
22 FTIR remote sensing observations, Atmos. Chem. Phys., 11, 6735-6748, 10.5194/acp-11-
23 6735-2011, 2011.
- 24 Feely, R. A., Sabine, C. L., Lee, K., Berelson, W., Kleypas, J., Fabry, V. J., and Millero, F. J.:
25 Impact of Anthropogenic CO₂ on the CaCO₃ System in the Oceans, Science, 305, 362-366,
26 10.1126/science.1097329, 2004.
- 27 Gurk, C., Fischer, H., Hoor, P., Lawrence, M. G., Lelieveld, J., and Wernli, H.: Airborne in-
28 situ measurements of vertical, seasonal and latitudinal distributions of carbon dioxide over
29 Europe, Atmos. Chem. Phys., 8, 6395-6403, 10.5194/acp-8-6395-2008, 2008.
- 30 Halloran, P. R.: Does atmospheric CO₂ seasonality play an important role in governing the
31 air-sea flux of CO₂?, Biogeosciences, 9, 2311-2323, 10.5194/bg-9-2311-2012, 2012.



- 1 Heinze, C., Maier-Reimer, E., and Winn, K.: Glacial pCO₂ Reduction by the World Ocean:
2 Experiments With the Hamburg Carbon Cycle Model, *Paleoceanography*, 6, 395-430,
3 10.1029/91PA00489, 1991.
- 4 Henne, S., Furger, M., and Prévôt, A. S. H.: Climatology of Mountain Venting-Induced
5 Elevated Moisture Layers in the Lee of the Alps, *JOURNAL OF APPLIED*
6 *METEOROLOGY*, 44, 620-633, 10.1175/JAM2217.1, 2005.
- 7 Henne, S., Brunner, D., Folini, D., Solberg, S., Klausen, J., and Buchmann, B.: Assessment of
8 parameters describing representativeness of air quality in-situ measurement sites, *Atmos.*
9 *Chem. Phys.*, 10, 3561-3581, 10.5194/acp-10-3561-2010, 2010.
- 10 Henne, S., Steinbacher, M., Mahieu, E., Bader, W., Blumenstock, T., Cuevas-Agulló, E.,
11 Brunner, D., and Buchmann, B.: Comparison of ground-based remote sensing and in-situ
12 observations of CO, CH₄ and O₃ accounting for representativeness uncertainty, EGU General
13 Assembly, Vienna, Austria, 7-12 April 2013, 2013.
- 14 Henne, S., D. Brunner, B. Oney, M. Leuenberger, W. Eugster, I. Bamberger, F. Meinhardt,
15 M. Steinbacher, and L. Emmenegger, Validation of Swiss Methane Emission Inventory by
16 Atmospheric Observations and Inverse Modelling, *Atmos. Chem. Phys. Discuss.*, 15, 35417-
17 35484, doi: 10.5194/acpd-15-35417-2015, 2015.
- 18 Heymann, J., Reuter, M., Hilker, M., Buchwitz, M., Schneising, O., Bovensmann, H.,
19 Burrows, J. P., Kuze, A., Suto, H., Deutscher, N. M., Dubey, M. K., Griffith, D. W. T., Hase,
20 F., Kawakami, S., Kivi, R., Morino, I., Petri, C., Roehl, C., Schneider, M., Sherlock, V.,
21 Sussmann, R., Velasco, V. A., Warneke, T., and Wunch, D.: Consistent satellite XCO₂
22 retrievals from SCIAMACHY and GOSAT using the BESD algorithm, *Atmos. Meas. Tech.*,
23 8, 2961-2980, 10.5194/amt-8-2961-2015, 2015.
- 24 IPCC: Climate Change 2013: The Physical Science Basis. Contribution of Working Group I
25 to the Fifth Assessment Report of the Intergovernmental Panel on Climate Change,
26 Cambridge University Press, Cambridge, United Kingdom and New York, NY, USA, 1535
27 pp., 2013.
- 28 Karl, T. R., and Trenberth, K. E.: Modern Global Climate Change, *Science*, 302, 1719-1723,
29 10.1126/science.1090228, 2003.



- 1 Keeling, C. D., Bacastow, R. B., Bainbridge, A. E., Ekdahl, C. A., Guenther, P. R.,
2 Waterman, L. S., and Chin, J. F. S.: Atmospheric carbon dioxide variations at Mauna Loa
3 Observatory, Hawaii, *Tellus*, 28, 538-551, 10.1111/j.2153-3490.1976.tb00701.x, 1976.
- 4 Keeling, C. D., Whorf, T. P., Wahlen, M., and van der Plichtt, J.: Interannual extremes in the
5 rate of rise of atmospheric carbon dioxide since 1980, *Nature*, 375, 666-670, 1995.
- 6 Keeling, C. D., Piper, S. C., Bacastow, R. B., Wahlen, M., Whorf, T. P., Heimann, M., and
7 Meijer, H. A.: Exchanges of Atmospheric CO₂ and ¹³CO₂ with the Terrestrial Biosphere and
8 Oceans from 1978 to 2000. I. Global Aspects, SIO Reference Series, No. 01-06, Scripps
9 Institution of Oceanography, San Diego, 88, 2001.
- 10 Komhyr, W. D., Gammon, R. H., Harris, T. B., Waterman, L. S., Conway, T. J., Taylor, W.
11 R., and Thoning, K. W.: GLOBAL ATMOSPHERIC CO₂ DISTRIBUTION AND
12 VARIATIONS FROM 1968-1982 NOAA GMCC CO₂ FLASK SAMPLE DATA, *J.*
13 *Geophys. Res.-Atmos.*, 90, 5567-5596, 10.1029/JD090iD03p05567, 1985.
- 14 Le Quéré, C., Peters, G. P., Andres, R. J., Andrew, R. M., Boden, T., Ciais, P., Friedlingstein,
15 P., Houghton, R. A., Marland, G., Moriarty, R., Sitch, S., Tans, P., Arneeth, A., Arvanitis, A.,
16 Bakker, D. C. E., Bopp, L., Canadell, J. G., Chini, L. P., Doney, S. C., Harper, A., Harris, I.,
17 House, J. I., Jain, A. K., Jones, S. D., Kato, E., Keeling, R. F., Klein Goldewijk, K.,
18 Körtzinger, A., Koven, C., Lefèvre, N., Omar, A., Ono, T., Park, G. H., Pfeil, B., Poulter, B.,
19 Raupach, M. R., Regnier, P., Rödenbeck, C., Saito, S., Schwinger, J., Segschneider, J.,
20 Stocker, B. D., Tilbrook, B., van Heuven, S., Viovy, N., Wanninkhof, R., Wiltshire, A.,
21 Zaehle, S., and Yue, C.: Global carbon budget 2013, *Earth Syst. Sci. Data Discuss.*, 6, 689-
22 760, 10.5194/essdd-6-689-2013, 2013.
- 23 Machida, T., Kita, K., Kondo, Y., Blake, D., Kawakami, S., Inoue, G., and Ogawa, T.:
24 Vertical and meridional distributions of the atmospheric CO₂ mixing ratio between northern
25 midlatitudes and southern subtropics, *Journal of Geophysical Research: Atmospheres*, 107,
26 8401, 10.1029/2001JD000910, 2002.
- 27 Machida, T., Matsueda, H., Sawa, Y., Nakagawa, Y., Hirotsu, K., Kondo, N., Goto, K.,
28 Nakazawa, T., Ishikawa, K., and Ogawa, T.: Worldwide Measurements of Atmospheric CO₂
29 and Other Trace Gas Species Using Commercial Airlines, *Journal of Atmospheric and*
30 *Oceanic Technology*, 25, 1744-1754, 10.1175/2008JTECHA1082.1, 2008.



- 1 Mahieu, E., Zander, R., Delbouille, L., Demoulin, P., Roland, G., and Servais, C.: Observed
2 Trends in Total Vertical Column Abundances of Atmospheric Gases from IR Solar Spectra
3 Recorded at the Jungfraujoch, *Journal of Atmospheric Chemistry*, 28, 227-243,
4 10.1023/A:1005854926740, 1997.
- 5 Messenger, C., Schmidt, M., Ramonet, M., Bousquet, P., Simmonds, P., Manning, A., Kazan,
6 V., Spain, G., Jennings, S. G., and Ciais, P.: Ten years of CO₂, CH₄, CO and N₂O fluxes over
7 Western Europe inferred from atmospheric measurements at Mace Head, Ireland, *Atmos.*
8 *Chem. Phys. Discuss.*, 8, 1191-1237, 10.5194/acpd-8-1191-2008, 2008.
- 9 Morino, I., Uchino, O., Inoue, M., Yoshida, Y., Yokota, T., Wennberg, P. O., Toon, G. C.,
10 Wunch, D., Roehl, C. M., Notholt, J., Warneke, T., Messerschmidt, J., Griffith, D. W. T.,
11 Deutscher, N. M., Sherlock, V., Connor, B., Robinson, J., Sussmann, R., and Rettinger, M.:
12 Preliminary validation of column-averaged volume mixing ratios of carbon dioxide and
13 methane retrieved from GOSAT short-wavelength infrared spectra, *Atmos. Meas. Tech.*, 4,
14 1061-1076, 10.5194/amt-4-1061-2011, 2011.
- 15 Oney, B., Henne, S., Gruber, N., Leuenberger, M., Bamberger, I., Eugster, W., and Brunner,
16 D.: The CarboCount CH sites: characterization of a dense greenhouse gas observation
17 network, *Atmos. Chem. Phys. Discuss.*, 15, 12911-12956, 10.5194/acpd-15-12911-2015,
18 2015.
- 19 Pales, J. C., and Keeling, C. D.: The concentration of atmospheric carbon dioxide in Hawaii,
20 *Journal of Geophysical Research*, 70, 6053-6076, 10.1029/JZ070i024p06053, 1965.
- 21 Pfister, G., Pétron, G., Emmons, L. K., Gille, J. C., Edwards, D. P., Lamarque, J. F., Attie, J.
22 L., Granier, C., and Novelli, P. C.: Evaluation of CO simulations and the analysis of the CO
23 budget for Europe, *Journal of Geophysical Research: Atmospheres*, 109, D19304,
24 10.1029/2004JD004691, 2004.
- 25 Pollock, R., Haring, R. E., Holden, J. R., Johnson, D. L., Kapitanoff, A., Mohlman, D.,
26 Phillips, C., Randall, D., Rechsteiner, D., Rivera, J., Rodriguez, J. I., Schwochert, M. A., and
27 Sutin, B. M.: The Orbiting Carbon Observatory instrument: performance of the OCO
28 instrument and plans for the OCO-2 instrument, 2010, 78260W-78260W-78213, 2010.
- 29 Rothman, L. S., Jacquemart, D., Barbe, A., Chris Benner, D., Birk, M., Brown, L. R., Carleer,
30 M. R., Chackerian, C., Chance, K., Coudert, L. H., Dana, V., Devi, V. M., Flaud, J.-M.,
31 Gamache, R. R., Goldman, A., Hartmann, J.-M., Jucks, K. W., Maki, A. G., Mandin, J.-Y.,



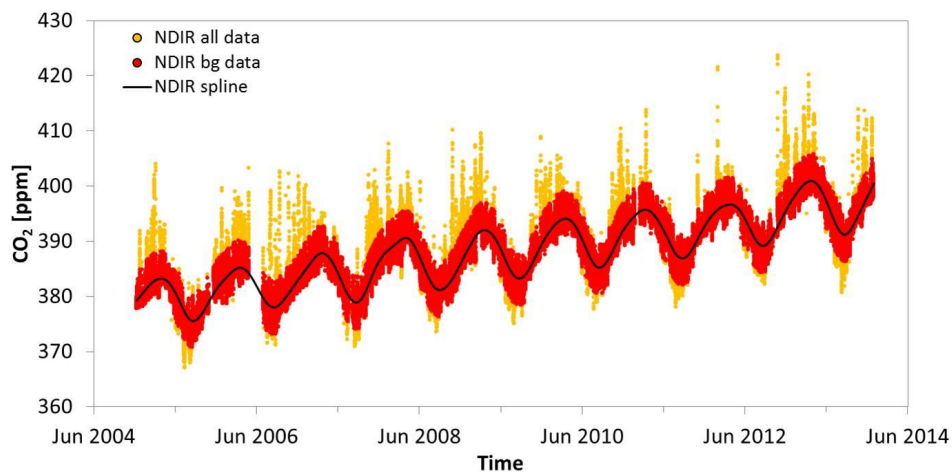
- 1 Massie, S. T., Orphal, J., Perrin, A., Rinsland, C. P., Smith, M. A. H., Tennyson, J.,
2 Tolchenov, R. N., Toth, R. A., Vander Auwera, J., Varanasi, P. and Wagner, G.: The
3 HITRAN 2004 molecular spectroscopic database, *Journal of Quantitative Spectroscopy and*
4 *Radiative Transfer*, 96(2), 139–204, doi:10.1016/j.jqsrt.2004.10.008, 2005.
- 5 Revelle, R., and Suess, H. E.: Carbon Dioxide Exchange Between Atmosphere and Ocean and
6 the Question of an Increase of Atmospheric CO₂ during the Past Decades, *Tellus*, 9, 18-27,
7 10.1111/j.2153-3490.1957.tb01849.x, 1957.
- 8 Sabine, C. L., Feely, R. A., Gruber, N., Key, R. M., Lee, K., Bullister, J. L., Wanninkhof, R.,
9 Wong, C. S., Wallace, D. W. R., Tilbrook, B., Millero, F. J., Peng, T.-H., Kozyr, A., Ono, T.,
10 and Rios, A. F.: The Oceanic Sink for Anthropogenic CO₂, *Science*, 305, 367-371,
11 10.1126/science.1097403, 2004.
- 12 Sillén, L. G.: Regulation of O₂, N₂ and CO₂ in the atmosphere; thoughts of a laboratory
13 chemist, *Tellus*, 18, 198-206, 10.1111/j.2153-3490.1966.tb00226.x, 1966.
- 14 Stohl, A., Forster, C., Frank, A., Seibert, P., and Wotawa, G.: Technical note: The Lagrangian
15 particle dispersion model FLEXPART version 6.2, *Atmos. Chem. Phys.*, 5, 2461-2474,
16 10.5194/acp-5-2461-2005, 2005.
- 17 Takahashi, T., Sutherland, S. C., Wanninkhof, R., Sweeney, C., Feely, R. A., Chipman, D.
18 W., Hales, B., Friederich, G., Chavez, F., Sabine, C., Watson, A., Bakker, D. C. E., Schuster,
19 U., Metzl, N., Yoshikawa-Inoue, H., Ishii, M., Midorikawa, T., Nojiri, Y., Körtzinger, A.,
20 Steinhoff, T., Hoppema, M., Olafsson, J., Arnarson, T. S., Tilbrook, B., Johannessen, T.,
21 Olsen, A., Bellerby, R., Wong, C. S., Delille, B., Bates, N. R., and de Baar, H. J. W.:
22 Climatological mean and decadal change in surface ocean pCO₂, and net sea–air CO₂ flux
23 over the global oceans, *Deep Sea Research Part II: Topical Studies in Oceanography*, 56, 554-
24 577, <http://dx.doi.org/10.1016/j.dsr2.2008.12.009>, 2009.
- 25 NOAA Earth System Research Laboratory, Global Monitoring Division:
26 <http://www.esrl.noaa.gov/gmd/ccgg/trends/>, access: 30.10.2014, 2014.
- 27 Schibig, M. F., Steinbacher, M., Buchmann, B., van der Laan-Luijkx, I. T., van der Laan, S.,
28 Ranjan, S., and Leuenberger, M. C.: Comparison of continuous in situ CO₂ observations at
29 Jungfraujoch using two different measurement techniques, *Atmos. Meas. Tech.*, 8, 57-68,
30 10.5194/amt-8-57-2015, 2015.



- 1 Tans, P. P., Fung, I. Y., and Takahashi, T.: Observational Constrains on the Global
2 Atmospheric CO₂ Budget, *Science*, 247, 1431-1438, 10.1126/science.247.4949.1431, 1990.
- 3 Thompson, D. R., Chris Benner, D., Brown, L. R., Crisp, D., Malathy Devi, V., Jiang, Y.,
4 Natraj, V., Oyafuso, F., Sung, K., Wunch, D., Castaño, R., and Miller, C. E.: Atmospheric
5 validation of high accuracy CO₂ absorption coefficients for the OCO-2 mission, *Journal of*
6 *Quantitative Spectroscopy and Radiative Transfer*, 113, 2265-2276,
7 <http://dx.doi.org/10.1016/j.jqsrt.2012.05.021>, 2012.
- 8 Thoning, K. W., Tans, P. P., and Komhyr, W. D.: Atmospheric carbon dioxide at Mauna Loa
9 Observatory: 2. Analysis of the NOAA GMCC data, 1974–1985, *Journal of Geophysical*
10 *Research: Atmospheres*, 94, 8549-8565, 10.1029/JD094iD06p08549, 1989.
- 11 Trolier, M., White, J. W. C., Tans, P. P., Masarie, K. A., and Gemery, P. A.: Monitoring the
12 isotopic composition of atmospheric CO₂: Measurements from the NOAA Global Air
13 Sampling Network, *Journal of Geophysical Research: Atmospheres*, 101, 25897-25916,
14 10.1029/96JD02363, 1996.
- 15 Uglietti, C., Leuenberger, M., and Brunner, D.: European source and sink areas of CO₂
16 retrieved from Lagrangian transport model interpretation of combined O₂ and CO₂
17 measurements at the high alpine research station Jungfraujoch, *Atmos. Chem. Phys.*, 11,
18 8017-8036, 10.5194/acp-11-8017-2011, 2011.
- 19 van der Laan-Luijkx, I. T., van der Laan, S., Uglietti, C., Schibig, M. F., Neubert, R. E. M.,
20 Meijer, H. A. J., Brand, W. A., Jordan, A., Richter, J. M., Rothe, M., and Leuenberger, M. C.:
21 Atmospheric CO₂, δ(O₂/N₂) and δ¹³CO₂ measurements at Jungfraujoch, Switzerland: results
22 from a flask sampling intercomparison program, *Atmos. Meas. Tech.*, 6, 1805-1815,
23 10.5194/amt-6-1805-2013, 2013.
- 24 Vigouroux, C., Blumenstock, T., Coffey, M., Errera, Q., García, O., Jones, N. B., Hannigan,
25 J. W., Hase, F., Liley, B., Mahieu, E., Mellqvist, J., Notholt, J., Palm, M., Persson, G.,
26 Schneider, M., Servais, C., Smale, D., Thölix, L. and De Mazière, M.: Trends of ozone total
27 columns and vertical distribution from FTIR observations at eight NDACC stations around
28 the globe, *Atmospheric Chemistry and Physics*, 15(6), 2915–2933, doi:10.5194/acp-15-2915-
29 2015, 2015.
- 30 Wunch, D., Toon, G. C., Blavier, J.-F. L., Washenfelder, R. A., Notholt, J., Connor, B. J.,
31 Griffith, D. W. T., Sherlock, V., and Wennberg, P. O.: The Total Carbon Column Observing



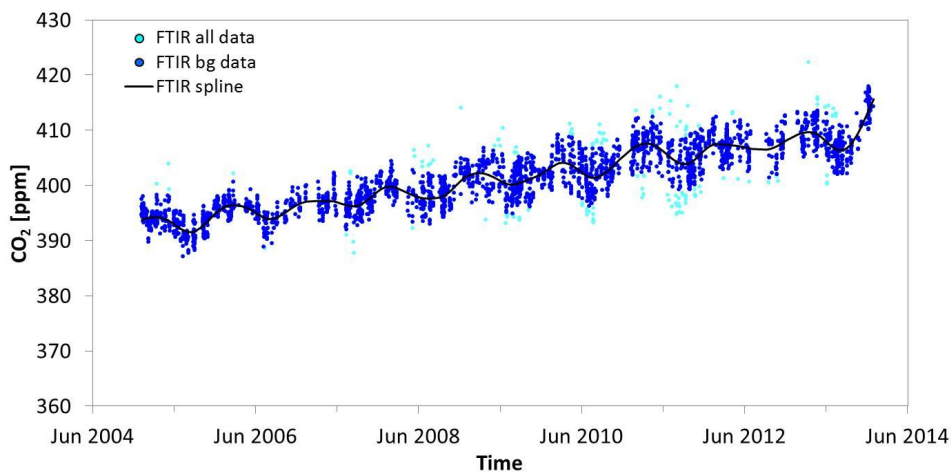
- 1 Network, Philosophical Transactions of the Royal Society of London A: Mathematical,
2 Physical and Engineering Sciences, 369, 2087-2112, 10.1098/rsta.2010.0240, 2011.
- 3 Yokota, T., Yoshida, Y., Eguchi, N., Ota, Y., Tanaka, T., Watanabe, H., and Maksyutov, S.:
4 Global Concentrations of CO₂ and CH₄ Retrieved from GOSAT: First Preliminary Results,
5 SOLA, 5, 160-163, 10.2151/sola.2009-041, 2009.
- 6 Zander, R., Mahieu, E., Demoulin, P., Duchatelet, P., Roland, G., Servais, C., Mazière, M. D.,
7 Reimann, S., and Rinsland, C. P.: Our changing atmosphere: Evidence based on long-term
8 infrared solar observations at the Jungfraujoch since 1950, Science of The Total Environment,
9 391, 184-195, <http://dx.doi.org/10.1016/j.scitotenv.2007.10.018>, 2008.
- 10 Zellweger, C., Ammann, M., Buchmann, B., Hofer, P., Lugauer, M., Rüttimann, R., Streit, N.,
11 Weingartner, E., and Baltensperger, U.: Summertime NO_y speciation at the Jungfraujoch,
12 3580 m above sea level, Switzerland, Journal of Geophysical Research: Atmospheres, 105,
13 6655-6667, 10.1029/1999JD901126, 2000.
- 14 Zellweger, C., Forrer, J., Hofer, P., Nyeki, S., Schwarzenbach, B., Weingartner, E., Ammann,
15 M., and Baltensperger, U.: Partitioning of reactive nitrogen (NO_y) and dependence on
16 meteorological conditions in the lower free troposphere, Atmos. Chem. Phys., 3, 779-796,
17 10.5194/acp-3-779-2003, 2003.
- 18 Zellweger, C., Hüglin, C., Klausen, J., Steinbacher, M., Vollmer, M., and Buchmann, B.:
19 Inter-comparison of four different carbon monoxide measurement techniques and evaluation
20 of the long-term carbon monoxide time series of Jungfraujoch, Atmos. Chem. Phys., 9, 3491-
21 3503, 10.5194/acp-9-3491-2009, 2009.
- 22 Zeng, N., Zhao, F., Collatz, G. J., Kalnay, E., Salawitch, R. J., West, T. O., and Guanter, L.:
23 Agricultural Green Revolution as a driver of increasing atmospheric CO₂ seasonal amplitude,
24 Nature, 515, 394-397, 10.1038/nature13893, 2014.
- 25



1

2 Figure 1. In-situ CO₂ mole fractions of the NDIR measurements as a function of time in ppm
3 at JFJ: All hourly averages before filtering (yellow), hourly averages after filtering (red) and
4 the spline (black line). Note that the yellow points correspond to only about 5 % of the whole
5 dataset.

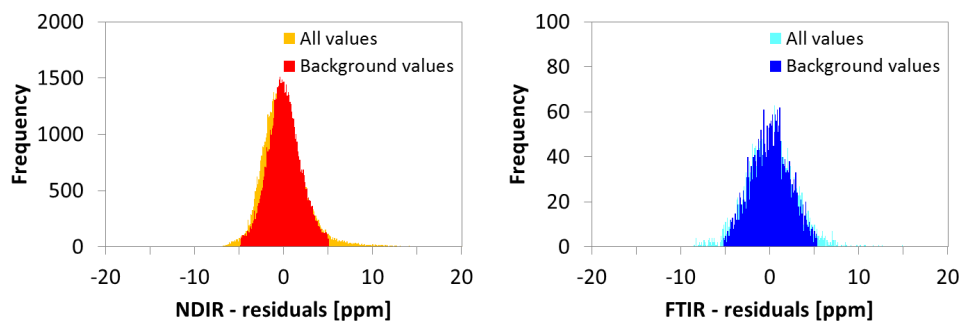
6



1

2 Figure 2. CO₂ mole fractions of the FTIR measurements as a function of time in ppm in the
3 column above JFJ: All hourly averages before filtering (light blue), hourly averages after
4 filtering (dark blue) and the spline (black line). The light blue points correspond to about 5 %
5 of the whole dataset.

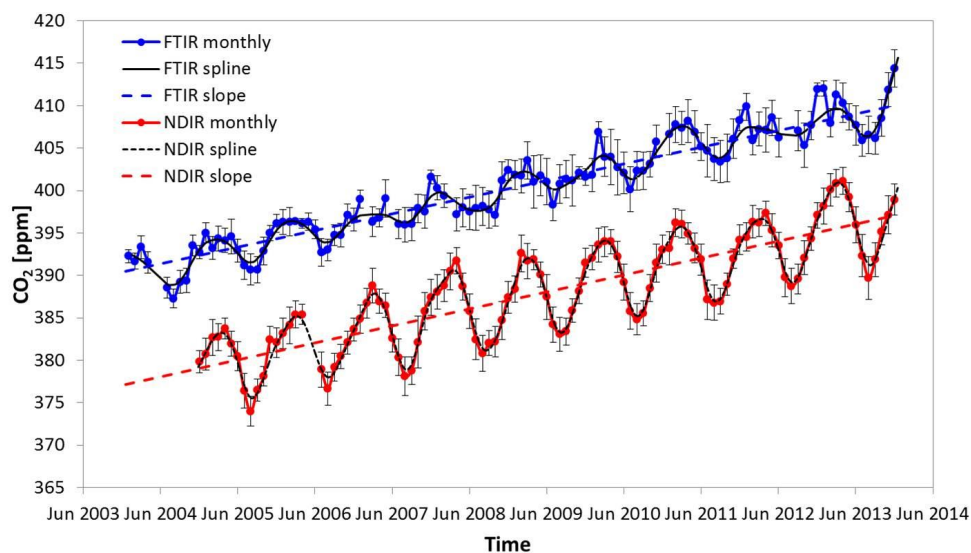
6



1

2 Figure 3. A: Histogram of the filtered NDIR residuals representing the background values
3 (red) of the in-situ measurements and the rejected values (black); B: Histogram of the filtered
4 FTIR residuals representing the background values (blue) of the column measurements and
5 the rejected values (black).

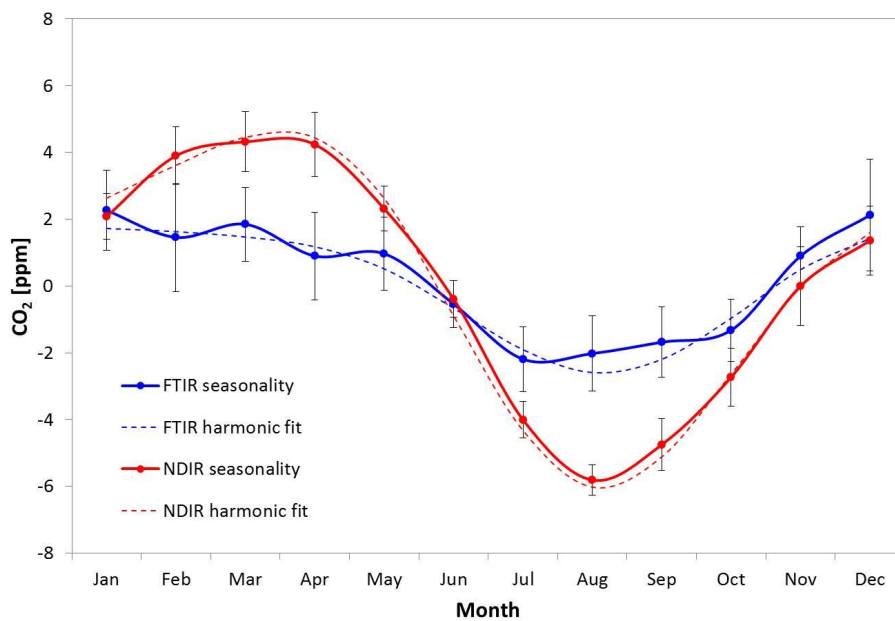
6



1

2 Figure 4. FTIR and NDIR CO₂ measurements at JFJ as a function of time: Monthly averages
3 of the filtered FTIR data (blue), spline (black line), the annual CO₂ increase calculated from
4 the filtered FTIR dataset (blue dashed line), monthly averages of the filtered NDIR data (red),
5 spline (black dotted line) and the annual CO₂ increase calculated from the filtered NDIR
6 dataset (red dashed line).

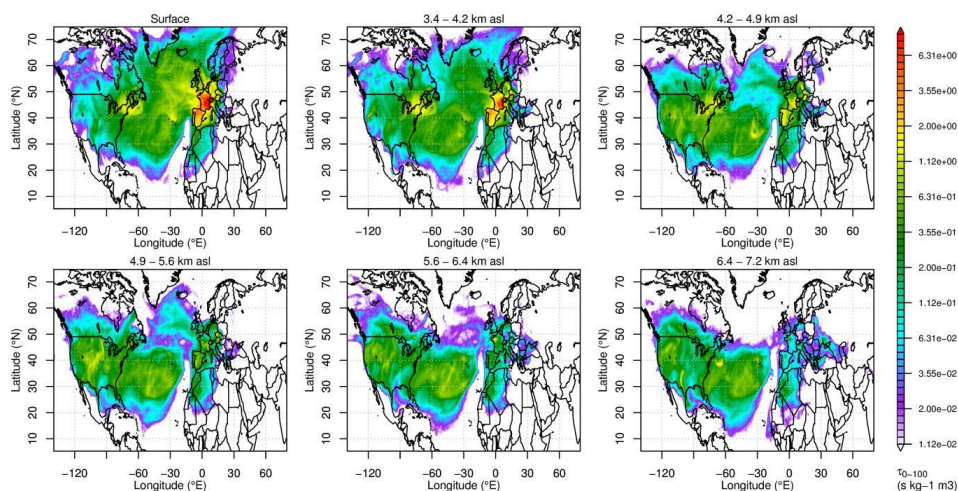
7



1

2 Figure 5. Monthly averaged seasonality of the filtered FTIR and NDIR CO₂ measurements for
3 the nine years of the comparison: averaged NDIR seasonality (red), two harmonic fit of the
4 NDIR seasonality (red dashed line), averaged FTIR seasonality (blue) and two harmonic fit of
5 the FTIR seasonality (dashed blue line).

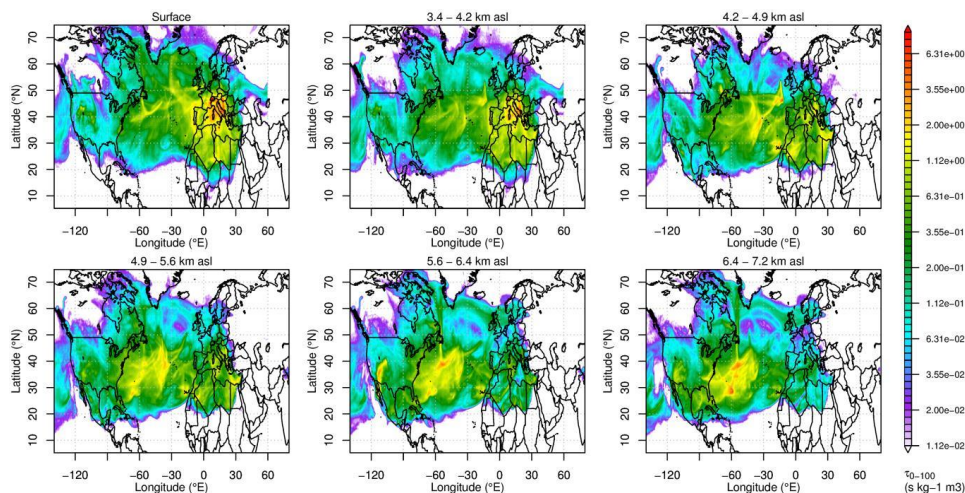
6



1

2 Figure 6. Surface source sensitivity (footprints) of the air masses at JFJ (surface in-situ) and in
3 the sub-columns above JFJ in August (CO_2 minimum of FTIR and NDIR time series) in the
4 period 2009 to 2011 simulated with FLEXPART. The height of the sub-columns is given
5 above the according subplots, the x-axis is the longitude, the y-axis represents the latitude, the
6 color code of the sensitivity is given at the right side.

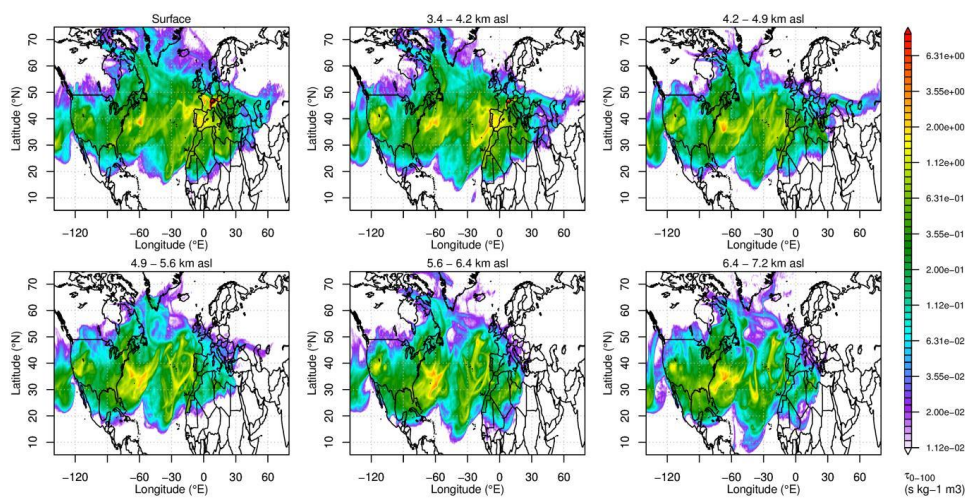
7



1

2 Figure 7. Surface source sensitivity (footprints) of the air masses at JFJ (surface in-situ) and
 3 in the sub-columns above JFJ in January (CO_2 maximum of the FTIR dataset) in the period 2009
 4 to 2011 simulated with FLEXPART. The height of the sub-columns is given above the
 5 according subplots, the x-axis is the longitude, the y-axis represents the latitude, the color
 6 code of the sensitivity is given at the right side.

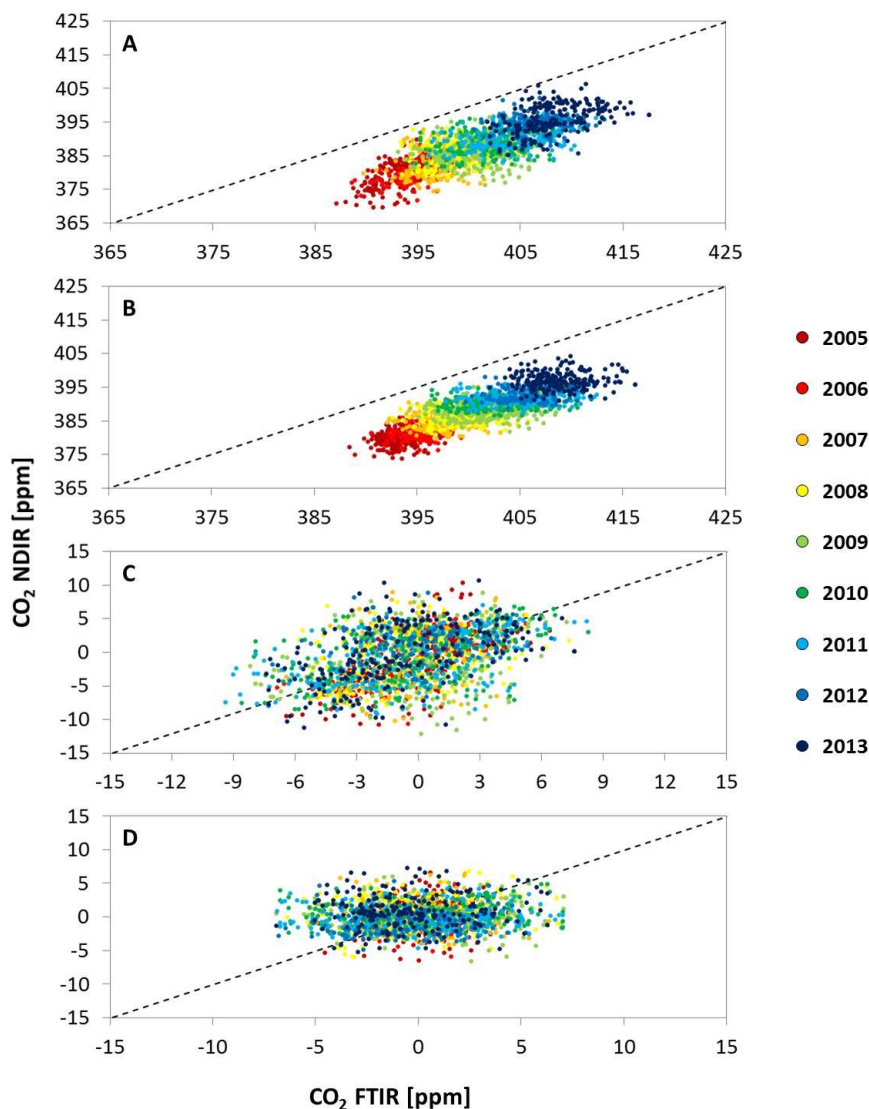
7



1

2 Figure 8. Surface source sensitivity (footprints) of the air masses at JFJ (surface in-situ) and
3 in the sub-columns above JFJ in March (CO_2 maximum of the NDIR dataset) in the period 2009
4 to 2011 simulated with FLEXPART. The height of the sub-columns is given above the
5 according subplots, the x-axis is the longitude, the y-axis represents the latitude, the color
6 code of the sensitivity is given at the right side.

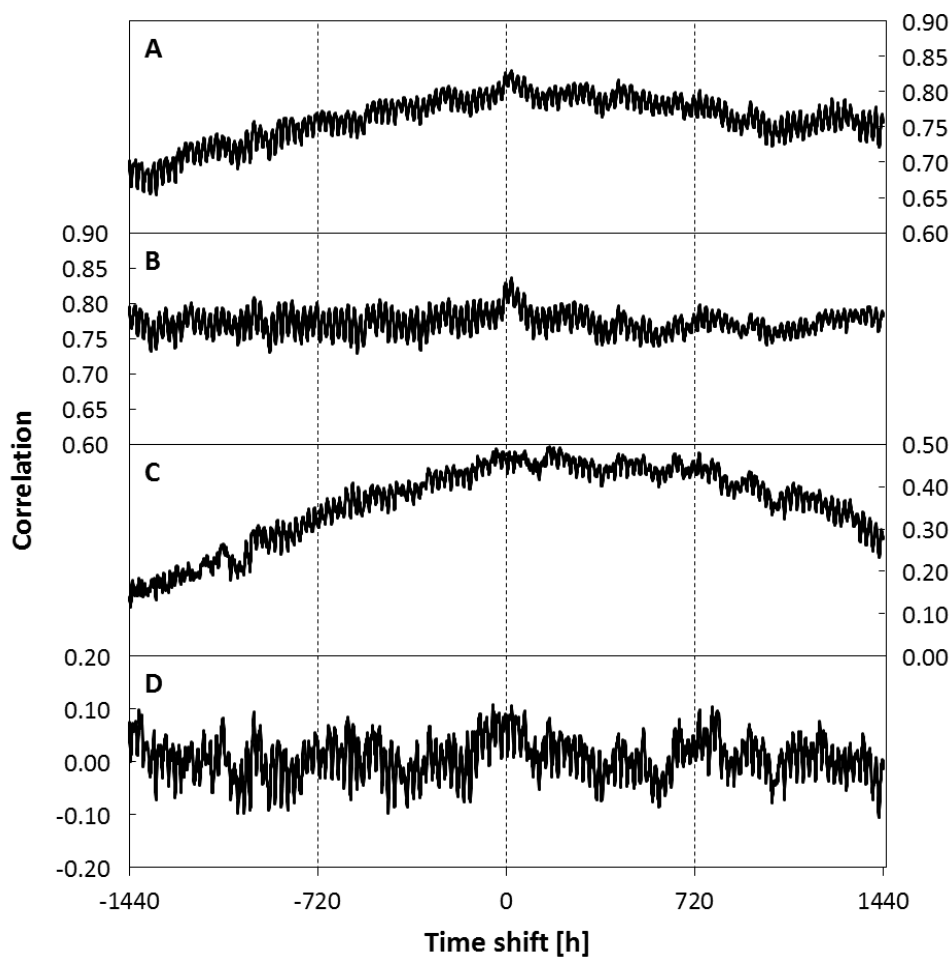
7



1

2 Figure 9. Correlation plots of the filtered hourly NDIR CO₂ measurements vs. the filtered
3 FTIR CO₂ measurements. The different colors refer to the years 2005 to 2013 (see legend). A:
4 The NDIR CO₂ measurements vs. FTIR CO₂ measurements including both, the annual CO₂
5 increase and the seasonality; B: As A but without seasonality; C: As A but detrended; D: As
6 A but with neither annual CO₂ increase nor seasonality. The dashed line is the 1:1 line.

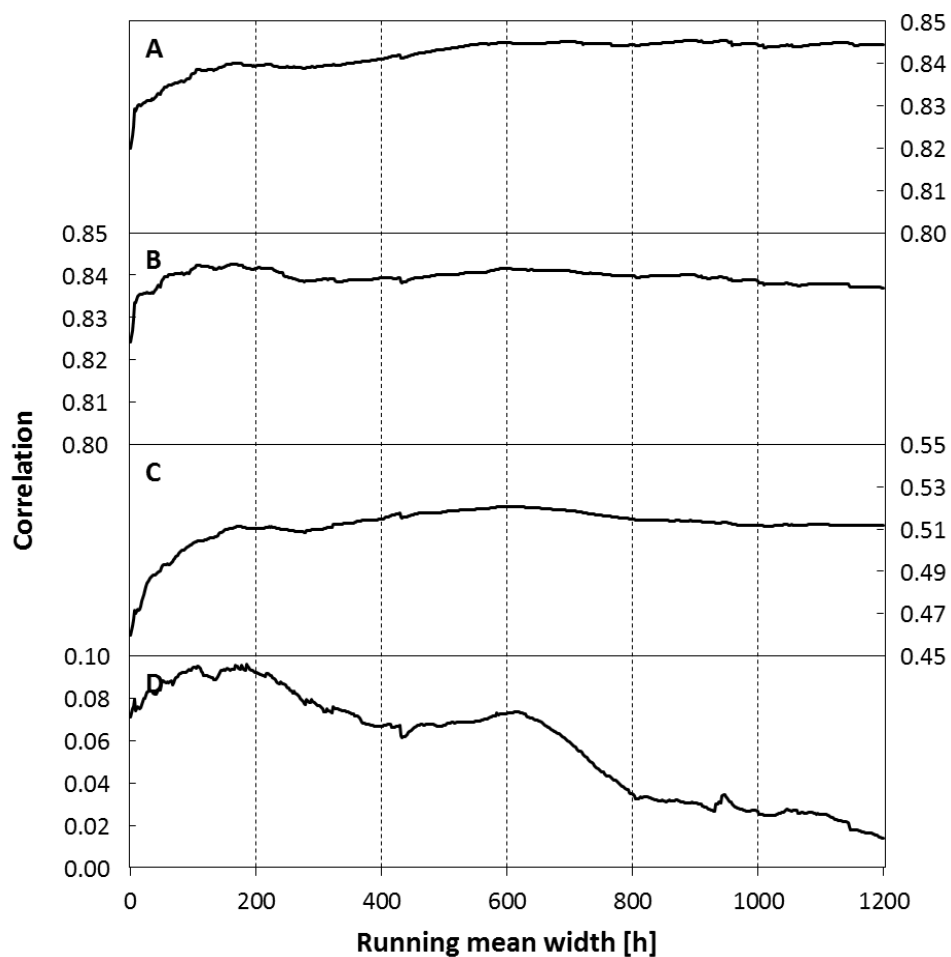
7



1

2 Figure 10. Evolution of the correlation between the filtered FTIR and NDIR datasets with
3 changing time shift. A: Correlation between complete datasets; B: Correlation between the
4 two datasets without seasonality; C: Correlation between the two datasets without trend; D:
5 Correlation between the two datasets with neither trend nor seasonality.

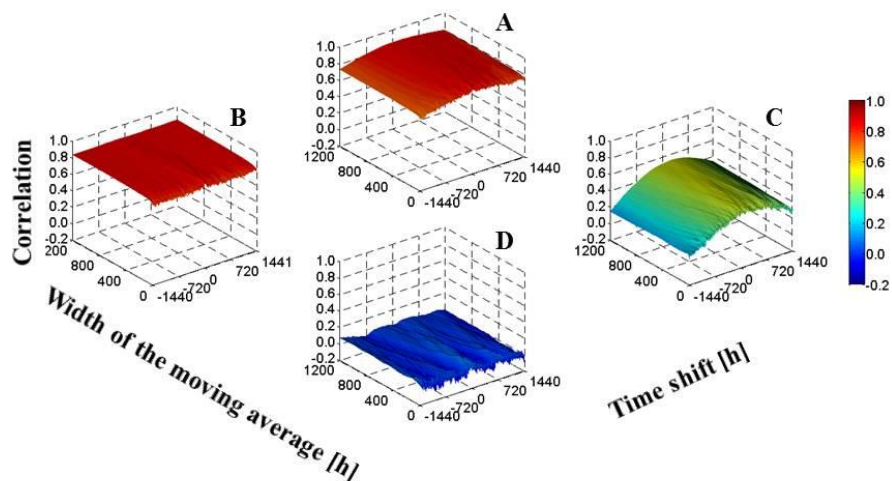
6



1

2 Figure 11. Change of the correlation between the filtered FTIR and NDIR datasets with
3 increasing width of the running mean. A: Correlation between the two datasets with
4 seasonality and slope; B: Correlation between the two datasets without seasonality; C:
5 Correlation between the two datasets without slope; D: Correlation between the two datasets
6 with neither slope nor seasonality.

7



1

2 Figure 12. Surface plots of the correlation of the NDIR CO₂ measurements vs. the FTIR CO₂
3 measurements. The x-axis corresponds to the time shift, the y-axis to the width of the moving
4 average and the z-axis to the correlation between the FTIR and the NDIR dataset, the color
5 code illustrates the correlation and corresponds to the z-axis values. A: The FTIR CO₂
6 measurements vs. the corresponding NDIR CO₂ measurements including the annual CO₂
7 increase as well as the seasonality; B: As A but without seasonality; C: As A but detrended;
8 D: As A but detrended and deseasonalized.